Size effect and localization in J2 plasticity

M. Cervera and M. Chiumenti

International Center for Numerical Methods in Engineering (CIMNE)

Technical University of Catalonia (UPC)

Edificio C1, Campus Norte, Jordi Girona 1-3, 08034 Barcelona, Spain.

Abstract

This paper studies the phenomenon of structural size effect and strain localization in J2 plasticity. Size effect is here understood as the change in the response of a given structure when the spatial dimensions are scaled up or down while the geometry and other relevant properties of the structure are preserved. The work exploits the advantages of the mixed displacement-pressure formulation in incompressible or quasi incomplessible situations. Elasto-J2-plastic constitutive behaviour with regularized softening is considered. Stability issues are discussed to ensure existance and uniqueness of the solution of the corresponding discrete finite element formulation. Numerical examples show that the formulation derived is able to solve a wide range of structural scales, including real life engineering applications. The results obtained do not suffer from spurious mesh dependence. Furthermore, the formulation includes the classical theories of perfect plasticity and linear fracture mechanics as limit cases.

1 Introduction

The question of how the load capacity of geometrically similar structures varies when scaling up or down their relative sizes has been a question of interest in structural mechanics from the very beginning of the discipline, and over the centuries.

Five hundred years ago, after conducting experiments on the strength of ropes of different lengths, Leonardo da Vinci concluded that the strength of the rope is inversely proportional to its length.

More than a hundred years later, in the XVII century, Galileo [1] rejected Leonardo's conclusions and, in doing so, he introduced the concept of stress. Galileo established that geometrically similar structures of increasing sizes L, subjected to increasing loads P, fail at the same *nominal stress*, defined for 3D scaling as

$$\sigma_N = P/L^2 \tag{1}$$

or $\sigma_N = P/bL$ for 2D scaling, b being the thickness. The work of Galileo is regarded as the first *deterministic scaling theory* of solid mechanics. Any departure from Galileo's law can be described as size effect on structural strength.

Towards the end of the same XVII century, Mariotte [2] repeated the work of Leonardo and established the basis for the *statistical theory of size effect* by observing that long ropes support the same load as short ones, unless they include a flaw in which they will break sooner than the shorter. In this work, statistical effects are not considered, and structural failure is assumed to be a deterministic phenomenon.

During the XVIII century, as continuum mechanics and the theory of elasticity developed, the nominal stress was identified with the maximum stress in the structure, and it became obvious that Galileo's law failed when stress singularities existed.

In 1921, A. A. Griffith [3], after performing experiments on the brittle fracture of glass sheets, introduced the first fracture mechanics theory, a basis for what we now know as *linear elastic fracture mechanics (LEFM)*. For Griffith, a crack becomes unstable when the elastic energy stored by the material around the tip of the existing crack is greater than the energy necessary for extending the crack.

This energy criterion is essentially different from Galileo's stress criterion. It has been experimentally verified and theoretically justified that the failure
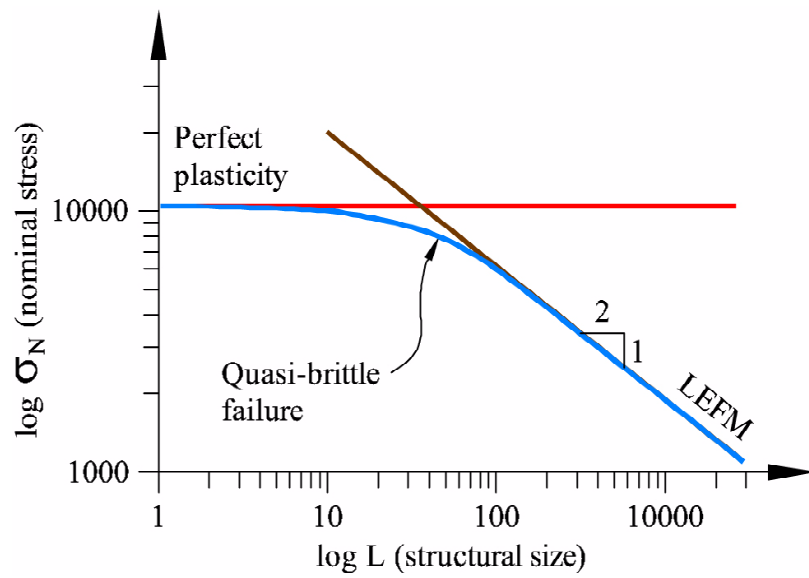
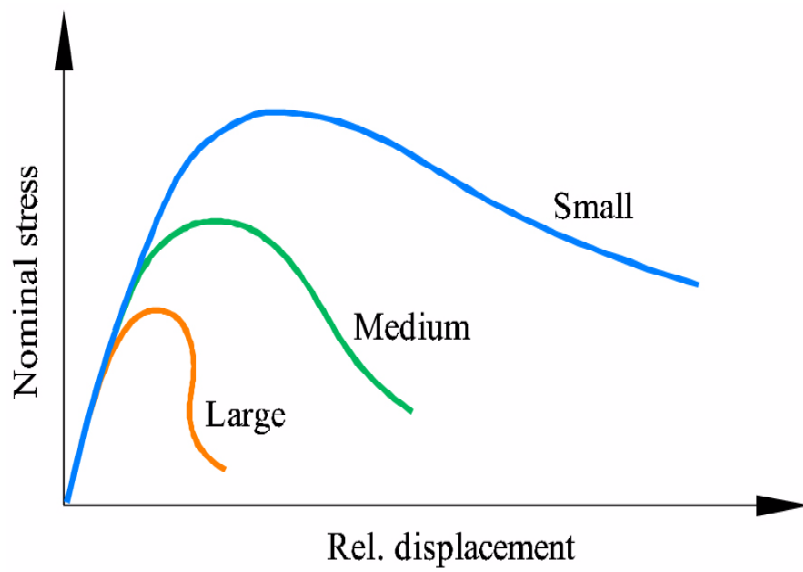Figure 1: Size effect on the nominal strength at failure

Figure 2: Size effect on the non linear structural response

3

nominal stress for failures with large crack or notches follows the law [4]:

$$\sigma_N = c\sigma_R(1 + L/L_R)^{-1/2} \qquad (2)$$

where σ_R is the nominal stress corresponding to a certain scale L_R (c is a constant).

Therefore, for almost a century there have been two very different approaches to assess structural failure. It is clear from their basic assumptions that the stress criterion is valid for very ductile failures, while the energy criterion is valid for very brittle behaviour. With regard to the scaling effect, experimental evidence shows that, for a given structural problem, ductile behaviour corresponds to the small scale limit, while brittle fracture occurs in large scale limit. More precisely, ductile behaviour is observed when the energy dissipated by inelastic behaviour in the formation of the failure mechanism is much larger than the total stored elastic energy; contrariwise, brittle behaviour occurs when the ratio between the dissipated inelastic and available elastic energies is close to one.

But, even if these considerations clarify the limits of applicability of both failure criteria, it is also true that real life engineering applications rarely correspond to one or the other of the limit situations. The small scale limit is suitable for small laboratory specimens, and the large scale limit is appropriate for structures of very large dimensions or even for scales larger than man-made structures. Thus, it is of practical interest to develop analytical and numerical tools suitable to bridge the gap between perfectly ductile and perfectly brittle behaviour. This is called *quasi-brittle failure*. Figure 1 shows the observed scale effect law for quasi-brittle behaviour, bridging in-between the two described limits. Note that the scales used in both axes of Figure 1 are logarithmic.

In quasi-brittle fracture, size effect does not only affect the load capacity (peak load), it also reflects on the post-peak behaviour (ductility) of the structure. Figure 2 shows curves of nominal stress vs. relative deflection for geometrically similar structures of different scale, properly normalized to make them comparable. Apart from the effect on the peak load, it is also evident that for small structures the post-peak curves descend slowly, for larger structures the descend is steeper, and for sufficiently large scale structures the response exhibits a snap-back, that is, the slope in the post-peak regime changes from negative to positive and becomes negative again. The areas under the load-deflection curves in Figure 2 characterize the energy absorp-

tion during the loading process. The capability of a quasibrittle structure to absorb energy decreases, in relative terms, as the structure size increases.

It is clear that tracking softening structural responses cannot be done under load control, experimentally or numerically. Therefore, the corresponding experiments or analyses are done under displacement control, a method capable of overcoming limit points (where the slope is zero). Unfortunately, displacement control fails near turning points (where the slope becomes infinite) and a combination of load and displacement control is necessary. Numerically this can be achieved by procedures such as the arc-length method.

In this work locally defined softening plasticity models are used to bridge the afore mentioned gap, covering the classical theories as limit cases. As model problem, J2-plasticity is selected as inelastic constitutive model, which corresponds to Mode II fracture in FM terminology. In this framework, structural failure is connected with the problem of *strain localization* and formation of *shear bands*.

Softening materials subjected to monotonic straining exhibit *strain localization*. In the so-called J2 materials, shear (or slip) strains concentrate. This phenomenon leads to the formation of *shear bands* inside the solid where the shear deformation concentrates while the material outside the band unloads. Upon continuing straining, the width of the shear band diminishes and, unless there is a physical limitation, it tends to zero. In J2 materials, these are called *slip lines*. It is generally accepted that the amount of energy released during the formation of a fracture unit area is a material property, called the *fracture energy*.

In the last two decades, many different finite element strategies have been devised to model strain localization and the references in the bibliography are innumerable. The possibilities are several, and both the weak and the strong discontinuity approaches have been followed. In the first, the objective is to capture the localization band as precisely as possible, with standard elements with continuous displacement interpolation. In the second, the displacement field is enhanced with discontinuous functions, defined either at element or nodal level, so that the limit discontinuous behavior can be captured. Regardless of the technical differences between the different discrete method proposed, as it is always possible to interpret a weak discontinuity as a regularization of a strong one, with the discontinuity smeared across the maximum possible resolution of the mesh, that is, one element, both approaches are essentially identical if the FE mesh is fine enough.

The main difficulty why most attempts to model weak discontinuities in

softening materials with standard, local, approaches fail is that the solutions obtained are spuriously determined by the fineness and orientation of the spatial discretization used. To remedy this, *micropolar, gradient-enhanced* and *non-local* models have been proposed in the last 25 years. In the micropolar strategy the standard non-polar description of Continuum Mechanics is substituted by other nonstandard theory, the Cosserat's continuum, see, for instance, [5] and [6]. In the gradient-enhanced strategy the nonlinear constitutive laws, for plasticity or damage, are made dependent not only on the local inelastic strain, but also on its second gradient, which is computed according to some additional relation which couples it to the local strain [7], [8], [9], [10], [11]. In the non-local strategy the standard format of the constitutive relationships (stress at a point depends on the strain at that point) is substituted by a non-local format (stress at a point depends on some average measure of the strain in the neighborhood of that point), see [7], [12], [13], [14], [15], among others. Even if these strategies have proved effective to some extend and a lot of research effort has been devoted to non-local models in the last years, these non-standard approaches pose new theoretical and computational difficulties, not fully mastered at the present moment.

Alternatively, significant research effort has been made to model numerically strong discontinuities directly. On one hand, the strong discontinuity approach (SDA, [16], [17], [18]) and, on the other, the extended finite element method (X-FEM, [19], [20], [21], [22]) allow to model strong discontinuities that progress through the FE mesh by enriching the nodal displacement degrees of freedom with additional ones that represent the displacement jumps. Also these computational procedures pose new computational challenges, as their application invariably needs the use of tracking algorithms in order to properly follow the progress of the strong discontinuity through the spatial mesh ([23], [24], [25]). It is not easy for these tracking algorithms to keep up with the development of multiple, interconnected or branching discontinuities.

Most of the studies about localization with J2 plasticity have been carried out using the irreducible formulation, with the displacement field as the only primary variable. Unfortunately, J2 plastic flow is isochoric, and the irreducible formulation is not well suited to cope with the incompressibility constraint. Even in compressible materials, for strain localization to take place, the plastic regime has to be well developed and, then, the (incompressible) plastic part of the deformation is dominant over the (compressible) elastic part. Displacement-based finite element methods may lead to inaccu-

rate numerical results in presence of constraints, such as in incompressibility or nearly incompressible situations. The unsuitability of the irreductible formulation is more evident if low order finite elements are used and, very especially, for simplicial elements (triangles and tetrahedra). The need to solve this difficulty is still today the drive for active research, see, for instance, reference [26].

Contrariwise, the mixed displacement/pressure ($\mathbf{u}/p$) formulation is an appropriate framework to tackle (quasi)-incompressible problems [27]. In fact, very promising results have been obtained in localization problems with J2 plasticity using this formulation together with remeshing techniques in [28] and [29] and in coupled dynamic problems in [30] and [31]. Nevertheless, it is very difficult to construct stable low order elements and, again, particularly, low order simplicial elements. This is another very attractive area of ongoing research, see references [32], [33], [34], [35], [36], [37], [38], [39], [40], [41], among others.

In previous works, the authors have applied *stabilization methods* ([42], [43], [44], [45], [46] and [47]) to the solution of incompressible elasto-plastic and damage problems with mixed displacement-pressure linear/linear simplicial elements. These stabilization procedures lead to a discrete problem which is fully stable, free of pressure oscillations and volumetric locking and, thus, results obtained are practically *mesh independent*. This translates in the achievement of two important goals: (a) the position and orientation of the localization band is independent of the directional bias of the finite element mesh and (b) the global post-peak load-deflection curves are independent of the size of the elements in the localization band.

The outline of the paper is as follows. In the next section, a *non-dimensional format* for the problem of quasi-brittle fracture in elasto-plastic problems with softening is identified. In Section 3, the mixed formulation for J2 plasticity is outlined. For softening plasticity, the necessary regularization of the softening modulus according to the size of the elements inside the localization band is discussed. Later, the corresponding boundary value problem is formulated. Strong and weak FE forms are presented. Both $Q1P0$ quadrilateral (bilinear displacement and constant pressure interpolations) and $P1P1$ triangular (equal linear displacement and linear pressure interpolations) elements are used. Finally, two numerical benchmarks are presented to assess the present formulation and to demonstrate its ability to appropriately model structural size effect in quasi-brittle fracture. In the present work we apply this methodology to the study of structural size-effect.

7

2   Dimensional analysis in quasi-brittle fracture

Size effect is one particular aspect of the broader field of *dimensional analysis*. Dimensional analysis is a conceptual tool often applied in physics and engineering to understand situations involving a mix of different kinds of physical quantities. It is routinely used by scientists and engineers to check the plausibility of derived equations and computations. It is also used to form reasonable hypotheses about complex situations that can be tested by experiments or by more developed theories of the phenomena. Dimensional analysis has played a major role in the last century, and it has been profusely used in engineering to interpret the results of reduced scale experimental models.

The keystone of dimensional analysis is the Buckingham Π theorem [48]. This theorem describes how every physically meaningful equation involving n variables can be equivalently rewritten as an equation of $n - m$ dimensionless parameters, where m is the number of fundamental dimensions used. Furthermore, and perhaps most importantly, it provides a method for computing these dimensionless parameters from the given variables. From a fundamental point of view, dimensional analysis and the Π theorem reflect the requirement that the laws of physics are independent of the units employed to measure the physical variables.

Let us apply this fundamental theorem to the problem of quasi-brittle failure in elasto-plastic materials with softening. Let us start with the governing equations for the *elastic* problem, stated as: given the elastic tensor $\mathbf{C}$ and prescribed body forces $\mathbf{f}$, find the displacement, $\mathbf{u}$, strain, $\boldsymbol{\varepsilon}$ and stress, $\boldsymbol{\sigma}$, fields, such that:

$$\nabla \cdot \boldsymbol{\sigma} + \mathbf{f} = \mathbf{0} \tag{3a}$$

$$\boldsymbol{\sigma} = \mathbf{C} : \boldsymbol{\varepsilon} \tag{3b}$$

$$\boldsymbol{\varepsilon} = \nabla^s \mathbf{u} \tag{3c}$$

These equations, subjected to appropriate Dirichlet and Neumann boundary conditions, must be satisfied in Ω, the open and bounded domain of $\mathbb{R}^{n_{\dim}}$ occupied by the solid in a space of $n_{\dim}$ dimensions.

In this format, the number of variables is $n = 3$, and we will consider force and length as fundamental dimensions, so that $m = 2$. According to the Π theorem, the problem may be rewritten as an equation of $n - m = 1$ dimensionless parameter. Selecting L as a representative length scale of the

problem, we define non-dimensional coordinates, $\hat{\mathbf{x}} = \mathbf{x}/L$, and displacements, $\hat{\mathbf{u}} = \mathbf{u}/L$, so that $\boldsymbol{\varepsilon} = \hat{\nabla}^s \hat{\mathbf{u}}$. Also, selecting $\mathcal{E}$ as an appropriate elastic modulus, we define non-dimensional stresses, $\hat{\boldsymbol{\sigma}} = \boldsymbol{\sigma}/\mathcal{E} = \hat{\mathbf{C}} : \nabla^s \hat{\mathbf{u}}$, where $\hat{\mathbf{C}} = \hat{\mathbf{C}}(\nu)$ is a non-dimensional tensor which depends only on Poisson's ratio. Finally, defining non-dimensional forces, $\hat{\mathbf{f}} = \mathbf{f}L/\mathcal{E}$, Eq. (3a) may be rewritten in the non-dimensional form:

$$\hat{\nabla} \cdot \hat{\boldsymbol{\sigma}} + \hat{\mathbf{f}} = \mathbf{0} \tag{4}$$

Therefore, Poisson's ratio plays the role of the sought non-dimensional parameter

$$\Pi_E = \nu \tag{5}$$

As Π_E does not depend on L, the elastic problem scales with the forces in the same way that $\hat{\mathbf{f}}$. Strains and stresses do not depend on the scale of the problem.

To include *plastic* behaviour, we consider the field of plastic strains, $\boldsymbol{\varepsilon}^p$, and redefine the non-dimensional stresses as $\hat{\boldsymbol{\sigma}} = \boldsymbol{\sigma}/\mathcal{E} = \hat{\mathbf{C}} : \left(\hat{\nabla}^s \hat{\mathbf{u}} - \boldsymbol{\varepsilon}^p \right)$. Details on the plastic model may be omitted, but it can be formulated stating a yield criterion in the form:

$$\Phi(\boldsymbol{\sigma}, r) = \|\boldsymbol{\sigma}\| - r = 0 \tag{6}$$

where $\|\cdot\|$ denotes an appropriate stress norm and r is a stress-like internal variable that controls hardening or softening behaviour and which depends on an appropriate norm of the plastic strains $r = r(\|\boldsymbol{\varepsilon}^p\|)$. Defining a second yielding dimensionless parameter

$$\Pi_Y = \frac{f}{\mathcal{E}} \tag{7}$$

where f is a relevant strength measure. Normalizing $\hat{r} = r/f$, we can write

$$\hat{\Phi}(\hat{\boldsymbol{\sigma}}, \hat{r}) = \|\hat{\boldsymbol{\sigma}}\| - \Pi_Y \hat{r} = 0 \tag{8}$$

For *perfect plasticity*, $\hat{r} = 1$, and, as Π_Y does not depend on L, the perfect plasticity problem scales in the same way as the elastic problem. For *hardening plasticity*, $\hat{r} = \hat{r}(\|\boldsymbol{\varepsilon}^p\|)$, does not depend on L either, and scaling properties remain unchanged.

Let us consider now the problem of quasi-brittle fracture in *softening plasticity*. In this case, when yielding occurs $\hat{r} = 1$ and, upon progressive loading,

$\hat{r}$ diminishes until, eventually, it vanishes. During the process, dissipation occurs in the form of plastic work, whose rate is defined as $\dot{\mathcal{W}}^p = \boldsymbol{\sigma} : \dot{\boldsymbol{\varepsilon}}^p$, so that, at a given time t, plastic work is $\mathcal{W}_t^p(\|\boldsymbol{\varepsilon}^p\|_t) = \int_0^t \dot{\mathcal{W}}^p dt$. Let us call $\mathcal{W}_\infty^p = \int_0^\infty \dot{\mathcal{W}}^p dt$, to the total amount of plastic work, attained when $\hat{r} \to 0$. We can redefine $\hat{r}$ as $\hat{r} = 1 - \mathcal{W}_t^p / \mathcal{W}_\infty^p$.

We may now introduce a third dimensionless parameter Π_B

$$\Pi_B = \frac{\mathcal{U}_o^e}{\mathcal{W}_\infty^p} \tag{9}$$

where $\mathcal{U}_o^e = (1/2) f^2 / \mathcal{E}$ is an appropriate part of the elastic energy stored per unit volume when yielding occurs. Now, the plastic criterion (8) may be written as

$$\hat{\Phi}\left(\hat{\boldsymbol{\sigma}}, \hat{\mathcal{W}}_t^p\right) = \|\hat{\boldsymbol{\sigma}}\| - \Pi_Y \left(1 - \Pi_B \hat{\mathcal{W}}_t^p\right) = 0 \tag{10}$$

where $\hat{r} = \hat{r}\left(\Pi_Y, \Pi_B, \hat{\mathcal{W}}_t^p\right)$ depends on Π_Y, Π_B and $\hat{\mathcal{W}}_t^p = \mathcal{W}_t^p / \mathcal{U}_o^e$.

But softening leads to *strain localization* and fracture. Let us assume that there is a material property $\mathcal{G}$, the fracture energy, that defines the energy dissipated *per unit area* when a fracture surface forms, and that the elastic energy of the structure is dissipated only through plastic work. Then, it is

$$\Pi_B = \frac{\mathcal{U}_o^e}{\mathcal{G}/L} = \frac{L}{\mathcal{L}} \tag{11}$$

and Π_B becomes a *size-dependent* measure of the *brittleness* of the problem. For $\Pi_B = 0$, behaviour is ductile like in perfect and hardening plasticity; for $\Pi_B \neq 0$, behaviour is brittle and energy dissipation controls the problem.

The length $\mathcal{L} = 2\mathcal{E}\mathcal{G} / f^2$ depends only on the material properties; for this reason, it is often called the *material characteristic length*. From definition (11), it is obvious that the brittleness of the problem depends on the ratio between the dimensions of the problem and this material characteristic length and, therefore, the problem becomes more brittle as it is scaled up. It is also clear that the effect of scaling up a given problem is exactly equivalent to that of scaling down the fracture energy in the same proportion.

Finally, consider that localization takes place in a band of width h, so that

$$\Pi_B = \frac{L}{\mathcal{L}} = \frac{h}{\mathcal{L}}\frac{L}{h} = \Pi_B^h \frac{L}{h} \tag{12}$$

The ratio $\Pi_B^h = h/\mathcal{L}$ defines the brittleness inside the band, while the ratio L/h defines the resolution (sharpness of the localization band related to the problem size.

3 Mixed formulation for J2 plasticity

3.1 J2 plasticity constitutive model

The stress tensor $\boldsymbol{\sigma}$ may then expressed as:

$$\boldsymbol{\sigma} = p\mathbf{1} + \mathbf{s} \tag{13}$$

where $p = \frac{1}{3}\operatorname{tr}\boldsymbol{\sigma}$ and $\mathbf{s} = \operatorname{dev}\boldsymbol{\sigma}$ are the volumetric and the deviatoric parts of the stress tensor, respectively. Correspondingly, the strain tensor $\boldsymbol{\varepsilon}$ is expressed as:

$$\boldsymbol{\varepsilon}(\mathbf{u}) = \frac{1}{3}\varepsilon_v\mathbf{1} + \mathbf{e} \tag{14}$$

where $\varepsilon_v = \operatorname{tr}\boldsymbol{\varepsilon}$ and $\mathbf{e} = \operatorname{dev}\boldsymbol{\varepsilon}$ are the volumetric and the deviatoric parts of the strain tensor, respectively. On the other hand, the constitutive equations are expressed as:

$$
\begin{aligned}
p &= K\varepsilon_v^e \tag{15a}\\
\mathbf{s} &= 2G\operatorname{dev}\boldsymbol{\varepsilon}^e = 2G\mathbf{e}^e \tag{15b}
\end{aligned}
$$

where ε_v^e and $\mathbf{e}^e$ are the *elastic* volumetric and the deviatoric strains, respectively; K is the bulk modulus and G is the shear modulus.

On the other hand, the elastic deviatoric strain tensor $\mathbf{e}^e$ is defined as:

$$\mathbf{e}^e = \mathbf{e} - \mathbf{e}^p \tag{16}$$

where $\mathbf{e}^p$ is the plastic strain tensor, which in J2 plasticity is purely deviatoric.

Box 1 summarizes the elasto-plastic model used in this work, accounting for isotropic softening. As usual, the *equivalent plastic strain* is defined as $\xi = \left(\sqrt{2/3}\right)\|\mathbf{e}^p\|$, and the *equivalent von Mises stress* is $s = \left(\sqrt{3/2}\right)\|\mathbf{s}\|$. With these definitions, the rate of plastic work is $\dot{\mathcal{W}}^p = \mathbf{s} : \dot{\mathbf{e}}^p = s\dot{\xi}$.

Notice in Box 1 that the isotropic softening variable $r = r(\xi)$ defines the current size of the yield surface, as it controls the value of the radius of the von Mises cylinder. Initially, when the equivalent plastic strain $\xi = 0, r$ is

equal to the initial flow stress σ_o. Along the softening regime, r diminishes and, for large value of the equivalent plastic strain, it vanishes.

The plastic multiplier $\dot{\gamma}$ is determined from the Kuhn-Tucker and consistency conditions:

$$\dot{\gamma} \geq 0 \qquad \Phi\left(\mathbf{s}, r\right) \leq 0 \qquad \dot{\gamma}\,\Phi\left(\mathbf{s}, r\right) = 0 \qquad (17\text{a})$$

$$\text{if } \Phi\left(\mathbf{s}, r\right) = 0 \ \text{ then } \ \dot{\gamma}\,\dot{\Phi}\left(\mathbf{s}, r\right) = 0 \qquad (17\text{b})$$

Details on how to efficiently integrate the J2-plastic constitutive model can be found in reference [49].

Box-1: J2-plastic constitutive model

1) Von Mises yield function, Φ:

$$\Phi\left(\mathbf{s}, r\right) = \sqrt{\tfrac{3}{2}}\,\|\mathbf{s}\| - r = s - r$$

2) Isotropic softening variable, r:

$$r = \begin{cases} \sigma_o\left(1 - H\left(\frac{\xi}{\xi_o}\right)\right) & 0 \leq \xi \leq \frac{\xi_o}{H} \\ 0 & \frac{\xi_o}{H} \leq \xi \leq \infty \end{cases} \quad \text{linear soft.}$$

$$r = \sigma_o \exp\left(-2H\left(\frac{\xi}{\xi_o}\right)\right) \qquad 0 \leq \xi \leq \infty \qquad \text{exp. soft.}$$

where ξ is the equivalent plastic strain, σ_o is the flow stress, $\xi_o = \sigma_o/2G$ and $H > 0$ is the softening coefficient.

3) Plastic evolution laws:

$$\dot{\mathbf{e}}^p = \dot{\gamma}\,\mathbf{n}$$
$$\dot{\xi} = \dot{\gamma}\sqrt{\tfrac{2}{3}}$$

where $\dot{\gamma}$ is the plastic multiplier and
$\mathbf{n} = \dfrac{\partial \Phi}{\partial \mathbf{s}} = \dfrac{\mathbf{s}}{\|\mathbf{s}\|}$ is the normal to the yield surface.

Also, the total *deviatoric* plastic work along the softening process is

$$\mathcal{W}_\infty^p = \int_{t=0}^{t=\infty} \dot{\mathcal{W}}^p dt = \int_0^\infty r\left(\xi\right) d\xi = \frac{\sigma_o^2}{2\left(2G\right)} \frac{1}{H} \tag{18}$$

both for linear or exponential softening. It has to be remarked that this value is equal to the area below the $r - \xi$ curve, that defines the softening response. Note that the isotropic softening variable can be expressed as $r = \sigma_o\left(1 - \mathcal{W}_t^p / \mathcal{W}_\infty^p\right).$

In order to apply the dimensional analysis of Section 2 to the present plasticity model, consider that $\mathcal{E} = 2G$, $f = \sigma_o$ and the elastic *deviatoric* energy at yielding is $\mathcal{U}_o^e = \left(1/2\right)\sigma_o^2 / 2G$.

Introducing the normalized variables $\hat{s} = s / \sigma_o$, $\hat{r} = r / \sigma_o$, $\hat{\xi} = \xi / \xi_o$ and defining $\hat{r} = 1 - \mathcal{W}_t^p / \mathcal{W}_\infty^p$, the model can be expressed as

$$\hat{\Phi}\left(\hat{\boldsymbol{\sigma}}, \hat{\mathcal{W}}_t^p\right) = \hat{s} - \Pi_Y \left(1 - \Pi_B \hat{\mathcal{W}}_t^p\right) = 0 \tag{19}$$

where $\Pi_B = \mathcal{U}_o^e / \mathcal{W}_\infty^p$ is the local brittleness number and the normalized plastic work, $\hat{\mathcal{W}}_t^p = \mathcal{W}_t^p / \mathcal{U}_o^e$, is expressed as a function of the normalized equivalent plastic strain:

$$\hat{\mathcal{W}}_t^p\left(\hat{\xi}\right) = \begin{cases} \hat{\xi} & 0 \leq \hat{\xi} \leq \frac{1}{\Pi_B} \\ 0 & \frac{1}{\Pi_B} \leq \hat{\xi} \leq \infty \end{cases} \quad \text{linear soft.} \tag{20a}$$

$$\hat{\mathcal{W}}_t^p\left(\hat{\xi}\right) = 1 - \exp\left(-2\Pi_B \hat{\xi}\right) \quad 0 \leq \hat{\xi} \leq \infty \quad \text{exp. soft.} \tag{20b}$$

3.2   FE softening regularization

If softening is considered, strain localization occurs. In finite elements solutions, strains tend to localize in a band that is only one element across, independently of the element size. Consequently, plastic dissipation localizes in a band of width $h = h_e$, where h_e is the *element characteristic length* of the elements in the band.

For a locally defined model such as the plastic model of the previous Section, if the softening parameter $H = \Pi_B$ and, consequently, the plastic work $\mathcal{W}_\infty^p$ are considered as material properties, FE results necessarily exhibit lack of objectivity, because upon mesh refinement, as element size tends to zero, no energy is dissipated in the failure process. Clearly, this is physically unacceptable.

This can be remedied by modifying the softening law in such a way that the energy dissipated over a completely degraded finite element be equal to a given value, which depends on the fracture energy of the material $\mathcal{G}$ and on the element characteristic length h_e ([50], [51], [52]) that defines the width of the localization band. In this work, the size of the element will be computed as $h_e^2 = A_e$ for quadrilateral elements.

The procedure, sketched in Figure 3, is as follows. The total energy dissipated during the fracture process per unit volume $\mathcal{D}$ is scaled for each element so that the equation

$$\mathcal{D}\,h = \mathcal{G} \quad \Longrightarrow \quad \mathcal{D} = \frac{\mathcal{G}}{h} \tag{21}$$

holds. For a plastic model, $\mathcal{D} = \mathcal{W}_\infty^p$, and, using Eqs. (18) and (20a), we have:

$$H = \Pi_B^h = \frac{\mathcal{U}_o^e}{\mathcal{G}\,/\,h} = \frac{h}{\mathcal{L}} \tag{22}$$

where the length $\mathcal{L} = (\mathcal{G}\,/\,\mathcal{U}_o^e)$ is the *material characteristic length*, which depends only on the material properties. Eq. (22) makes the non-dimensional softening modulus $H = \Pi_B^h$ dependent on the ratio between the element and the material characteristic lengths.

Because of Eq. (21), the necessary condition $\mathcal{W}_\infty^p \geq \mathcal{U}_o^e$ requires that $H = \Pi_B^h \leq 1$. This condition sets a maximum size for the elements that can be used in the analysis, $h \leq \mathcal{L}$.
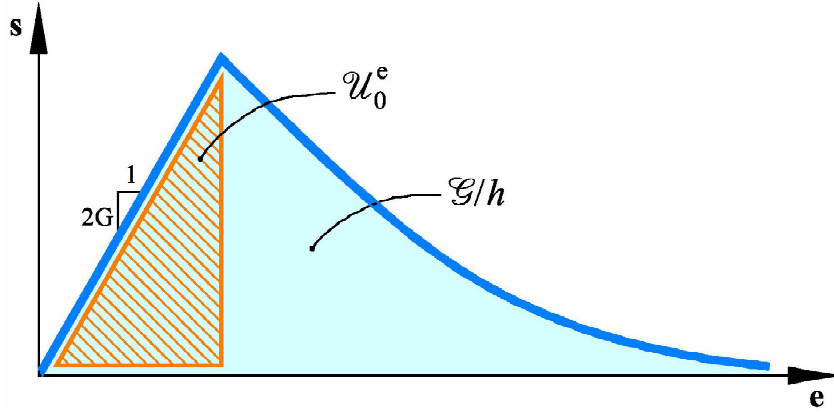

Figure 3: Softening regularization procedure based on elemental energy dissipation

14

Π_B^h is the *element (local) brittleness parameter*. It can be related to the global brittleness number of the problem using Eq.. (12):

$$\Pi_B = \Pi_B^h \frac{L}{h} \qquad (23)$$

that clearly reflects the phenomenon of size effect at structural level and its relation with the FE regularization.

4   Boundary value problem

Alternatively to Eq. (3a), the strong form of the continuum mechanical problem can be stated, in mixed form, as: for given prescribed body forces $\mathbf{f}$, find the displacement field $\mathbf{u}$ and the pressure field p, such that:

$$\nabla \cdot \mathbf{s} + \nabla p + \mathbf{f} = \mathbf{0} \qquad \text{in } \Omega \qquad (24a)$$

$$\nabla \cdot \mathbf{u} - \frac{1}{K} p = 0 \qquad \text{in } \Omega \qquad (24b)$$

where Ω is the domain occupied by the elasto-plastic solid. Eqs. (24a)-(24b) are subjected to appropriate Dirichlet and Neumann boundary conditions.

The associated *discrete* finite element weak form of the problem is [58]:

$$\left(\nabla^s \mathbf{v}_h, \mathbf{s}_h\right) + \left(\nabla \cdot \mathbf{v}_h, p_h\right) - \left(\mathbf{v}_h, \mathbf{f}\right) - \left(\mathbf{v}_h, \overline{\mathbf{t}}\right)_{\partial\Omega_t} = 0 \qquad \forall \mathbf{v}_h \quad (25a)$$

$$\left(q_h, \nabla \cdot \mathbf{u}_h\right) - \left(q_h, \frac{1}{K} p_h\right) = 0 \qquad \forall q_h \quad (25b)$$

where $\mathbf{u}_h$, $\mathbf{v}_h \in \mathcal{V}_h$ and p_h, $q_h \in \mathcal{Q}_h$ are the *discrete* displacement and pressure fields and their variations, defined onto the finite element spaces $\mathcal{V}_h$ and $\mathcal{Q}_h$, respectively.

In incompressible elasticity, K tends to infinity and, thus, the volumetric part of the elastic deformation vanishes. Additionally, in incompressible (J2) plasticity, the volumetric part of plastic deformation is also zero, so that $\varepsilon_v = \nabla \cdot \mathbf{u} = 0$. Therefore, the second terms in Eqs. (24b) and (25b) vanish.

A major difficulty when using the standard Galerkin discrete form (25a)-(25b) is that the BB-condition [53] for stability poses severe restrictions on the choice of the spaces $\mathcal{V}_h$ and $\mathcal{Q}_h$. For instance, standard mixed elements with continuous equal order linear/linear interpolation for both fields are not stable, and the lack of stability shows as uncontrollable oscillations in

the pressure field that usually, and very particularly in non linear problems, pollute the solution entirely.

Fortunately, the strictness of the BB-condition can be circumvented by modifying the discrete variational form appropriately, in order to attain the necessary global stability with the desired choice of interpolation spaces ([54], [55]). A particularly appealing consistent stabilization method is the *orthogonal sub-grid scale method (OSGS)*, originally developed for computational incompressible fluid mechanics problems ([56], [57]).

The OSGS stabilization method has been applied to the problem of incompressible elasto-plasticity, in small and finite strains, and continuum damage mechanics by the authors in previous works and the interested reader is referred to them for a detailed explanation, see [42], [43], [44], [45], [46] and [47]. These developments show that it is possible to stabilize in a consistent way the behaviour of mixed elements with continuous equal order interpolation. In particular, triangular 3-node *P1P1* elements, with linear/linear interpolations, can be used, displaying satisfactory stable behaviour.

An alternative to the use of stabilized mixed elements with continuous pressure interpolation is the use of pressure interpolation which is discontinuous between elements. In this case, Eq. (25b) may be solved at element level and the resulting pressure field is then substituted into Eq. (25a). This results in a global problem with only displacements as dofs. The implementation of such a procedure is very simple in a standard FE code.

Probably, the most popular of the mixed elements with discontinuous pressure is the *Q1P0* quadrilateral, with bilinear interpolation for displacements and constant pressure. Despite the fact that this element violates the BB-condition, optimal rate of convergence can be proven under suitable assumptions [58]; it can be said that *Q1P0* is marginally stable. Unfortunately, its performance degrades in irregular unstructured meshes.

5   Numerical results

The formulation presented in the preceding sections is illustrated below in two selected benchmark problems. The examples involve *incompressible* elasticity and J2-plasticity with exponential *softening*. The following material properties are assumed: Young's modulus $E = 10$ MPa, Poisson's ratio $\nu = 0.499$ (recall that $G = E/2\,(1+\nu)$, $K = E/3\,(1-2\nu)$), uniaxial yield stress $\sigma_o = E/1000 = 10$ KPa and mode II fracture energy $\mathcal{G} = 100$ J/m^2.

A cylindrical arc-length procedure, combined with the Newton-Raphson method, is used to solve the non-linear system of equations arising from the spatial and temporal discretization of the problem. An automatic procedure to decide the step size is used and about 200 steps are necessary to complete the analyses. Convergence of a time step is attained when the ratio between the norms of the residual and the total forces is lower than 10^{-2} %.

Calculations are performed with an enhanced version of the finite element program COMET [59], developed by the authors at the International Center for Numerical Methods in Engineering (CIMNE). Pre and post-processing is done with GiD, also developed at CIMNE [60].

5.1 Perforated strip

The first example is a plane-strain perforated strip loaded with a uniformly distributed axial load applied at both ends. Because of the double symmetry, only one quarter of the domain (the top right quarter) needs to be discretized. Figure 4a depicts the geometry of the problem; dimensions are related to length $r = 0.1$ m. The brittleness parameter of Eq. (11) is computed with $L = 10r$.
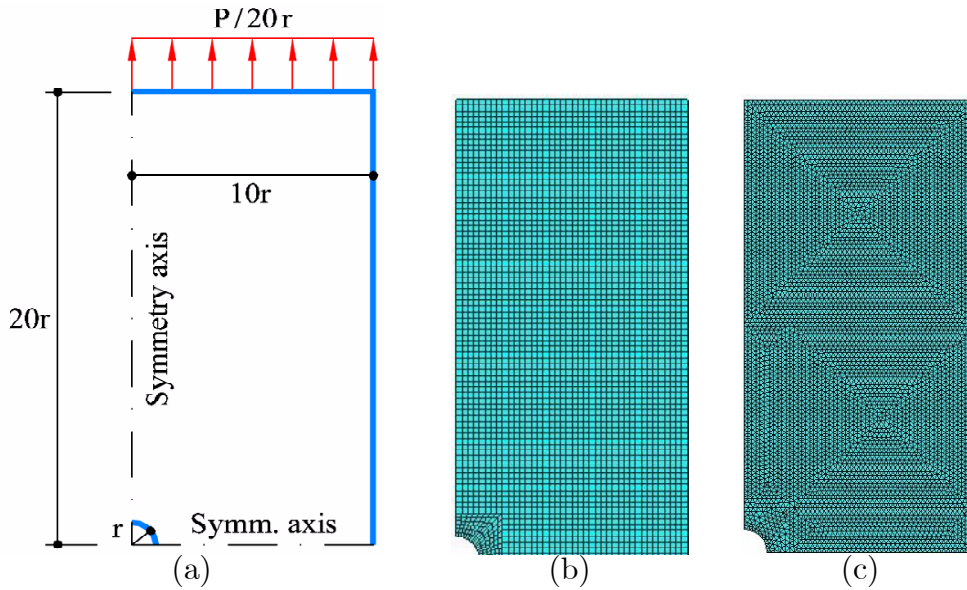

Figure 4: (a) Geometry, (b) structured Q1P0 and (c) unstructured P1P1 FE meshes used for the perforated strip
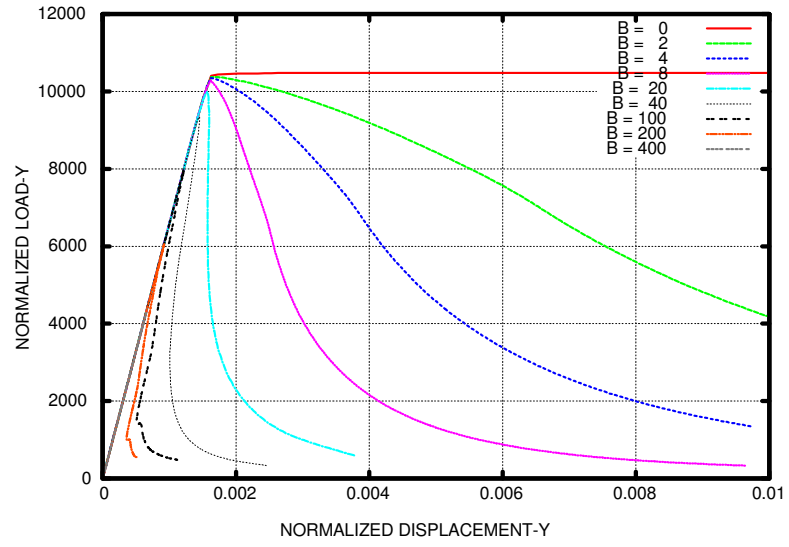
17

Figure 5: Nominal stress vs normalized top displacement curve for perforated strip with different scales
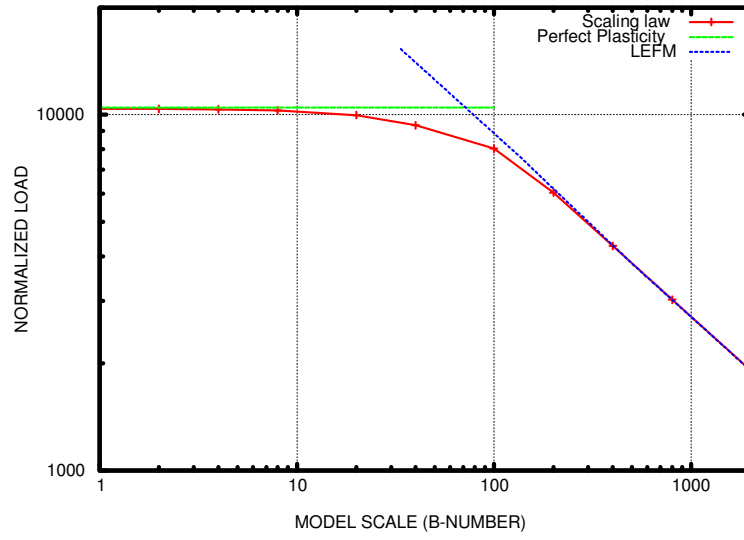

Figure 6: Size effect on the nominal strength at failure for perforated strip
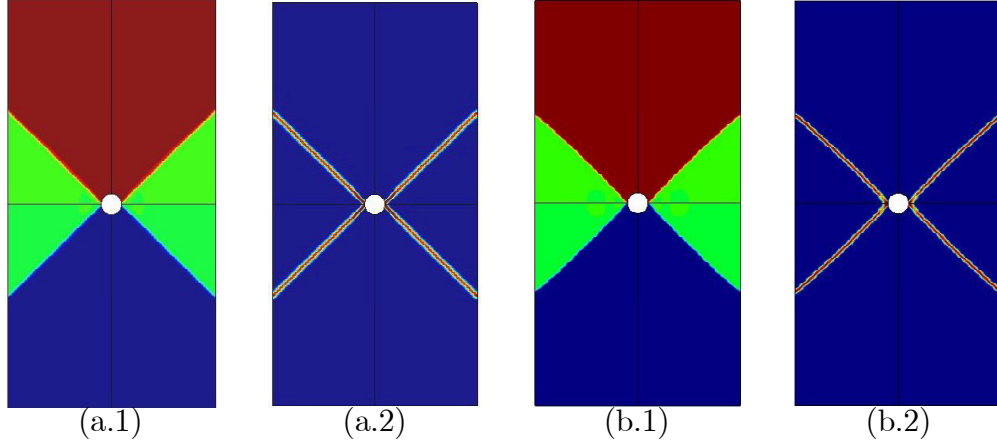
18

Figure 7: Results for perforated strip. Contours for: (a.1) vertical displacement and (a.2) equivalent plastic strain in Q1P0 mesh; (b.1) vertical displacement and (b.2) equivalent plastic strain in P1P1 mesh

Figure 4b shows the first mesh used in the analysis; it consists of 3,232 *Q1P0* quadrilaterals (3,359 nodes). Notice that the mesh is structured and most of the element sides are at 0° or 90° with the horizontal axis.

Figure 5 shows nominal stress vs normalized top-displacement curves (1 m thickness is assumed) obtained with different scales, from $\Pi_B = 0$ to $\Pi_B = 400$. For the smallest scale, $\Pi_B = 0$, behaviour is perfectly ductile and no softening occurs in the post-peak regime. On the other extreme, for the largest scale, $\Pi_B = 400$, the behaviour is almost perfectly brittle and the elastic loading branch nearly doubles back on itself. For intermediate increasing scales the normalized curves show increasing brittleness. For scales such that $\Pi_B > 20$, the curve snaps back and mixed load-displacement control is necessary.

Size effect on the structural strength of the perforated strip is demonstrated in Figure 6, which shows normalized peak load vs size in log scale. It is clear that the numerical solutions behave exactly as expected: for the smaller scales, the nominal stress is constant, as predicted by Galileo's scaling law, while for the largest scales, the nominal stress decreases according to the slope 1:-2 predicted by LEFM. It is most remarkable that the numerical solutions bridge the gap between these two limit theories smoothly.

Figure 7a shows results obtained for scale corresponding to $\Pi_B = 4$, once the plastic flow is fully developed and the collapse mechanism can be appreciated. The Figure shows contours for: (a.1) vertical displacement and

(a.2) equivalent deviatoric plastic strain. These plots demonstrate that the solution obtained corresponds to the analytical solution: a shear band that starts in the horizontal symmetry axis, where there is a mild stress concentration, and progresses across the specimen at approx.. 45° with the dominant field of vertical principal stresses. Orientation of the slip band is independent of the FE mesh used and the resolution is optimal: one element across. The solution is completely free of spurious pressure oscillations.

It has to be remarked that the deformation pattern and collapse mechanism computed for all the scales are identical.

In order to assess the validity of the solutions obtained, the problem is also solved using a second FE mesh, shown in Figure 4c ; it consists of 7,234 *P1P1* triangles (3,740 nodes). Notice that the mesh is totally unstructured and it does not show any directional bias.

Figure 7b shows results obtained using this second mesh for scale corresponding to $\Pi_B = 4$, once the collapse mechanism can be appreciated. This Figure shows contours for: (b.1) vertical displacement and (b.2) equivalent deviatoric plastic strain. It is evident that the solution obtained resembles closely the one obtained using the first mesh. This concordance stresses the consistency of the formulation presented.
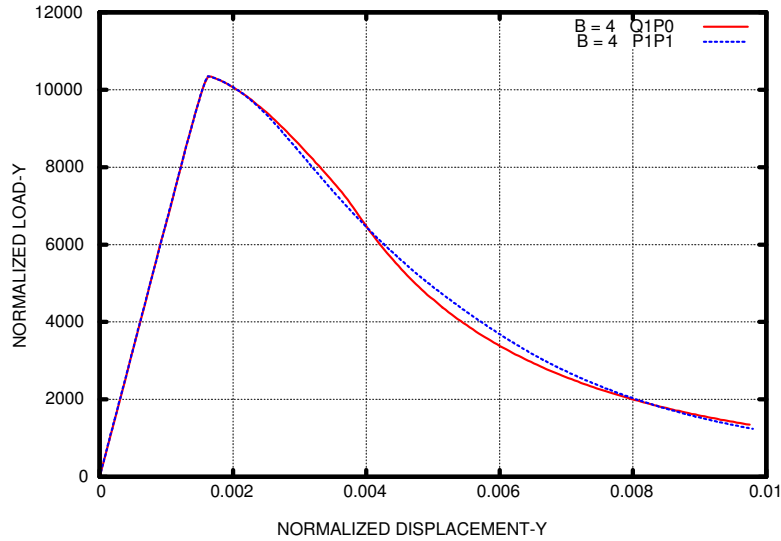

Figure 8: Nominal stress vs normalized top displacement curve for perforated strip with different meshes ($\Pi_B = 4$).

Finally, Figure 8 compares the nominal stress vs normalized top-displacement curves obtained with the two different meshes. The coincidence of the peak loads obtained and the similarity of the post-peak branch is remarkable.

5.2 Prandtl's punch test

The second example is the Prandtl's punch test, a well-known plane-strain 2D problem often used in the literature to test the ability of J2-plastic models to capture collapse loads and mechanisms. Figure 9a depicts the geometry of the problem, a rigid footing with a central point load; dimensions are related to length $b = 0.5$ m. The brittleness parameter of Eq. (11) is computed with $L = 2b$.

Because of the symmetry, only half of the domain (the right half) needs to be discretized. Figure 9b also shows the first mesh used in the analysis: 6,600 *Q1P0* quadrilaterals (6,771 nodes). Notice that the mesh is structured and all of the element sides are at 0° or 90° with the horizontal axis.

Figure 10 shows nominal stress vs normalized top displacement curves (1 m thickness is assumed) obtained with different scales, from $\Pi_B = 0$ to $\Pi_B = 200$. As in the previous example, for the smallest scale, $\Pi_B = 0$, behaviour is perfectly ductile and no softening occurs in the post-peak regime. For the largest scale, $\Pi_B = 200$, the behaviour is very brittle. For intermedi-
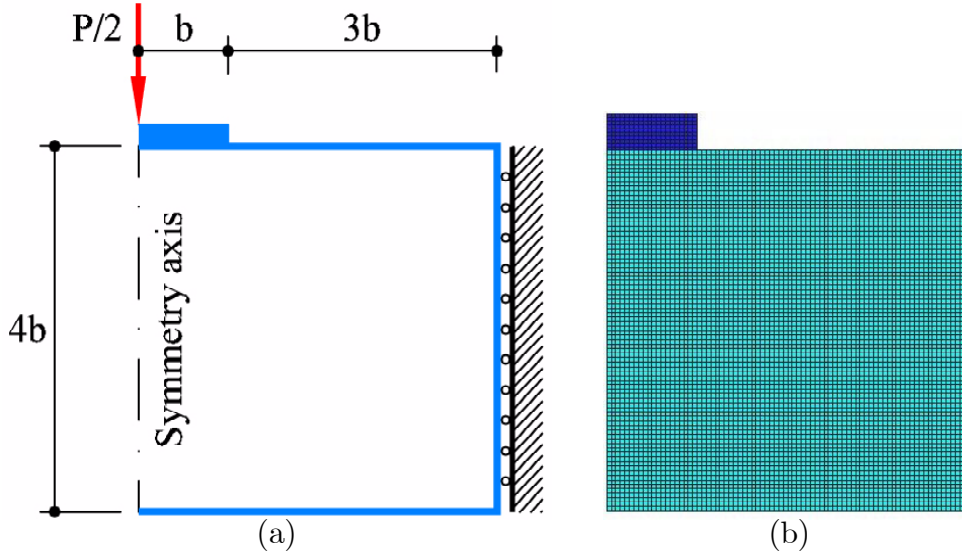

Figure 9: Geometry (a) and mesh (b) used for the 2D Prandtl's punch test
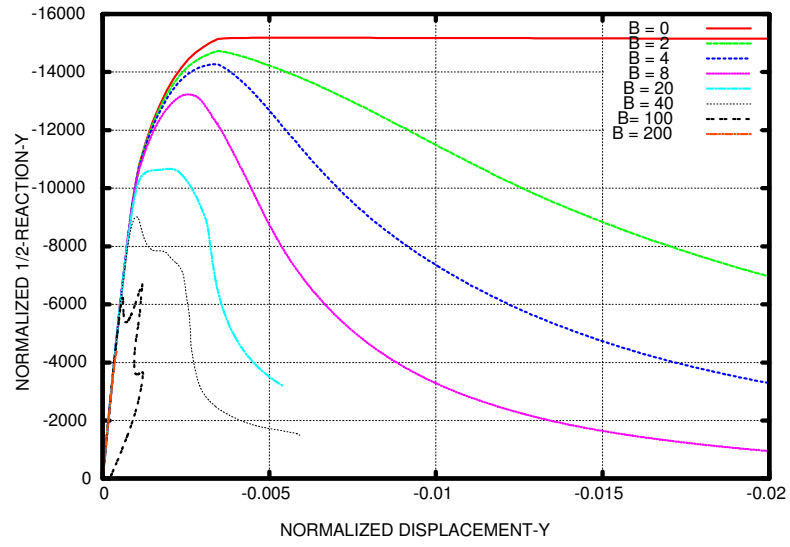
Figure 10: Nominal stress vs normalized top displacement curve for Prandtl's punch test with different scales
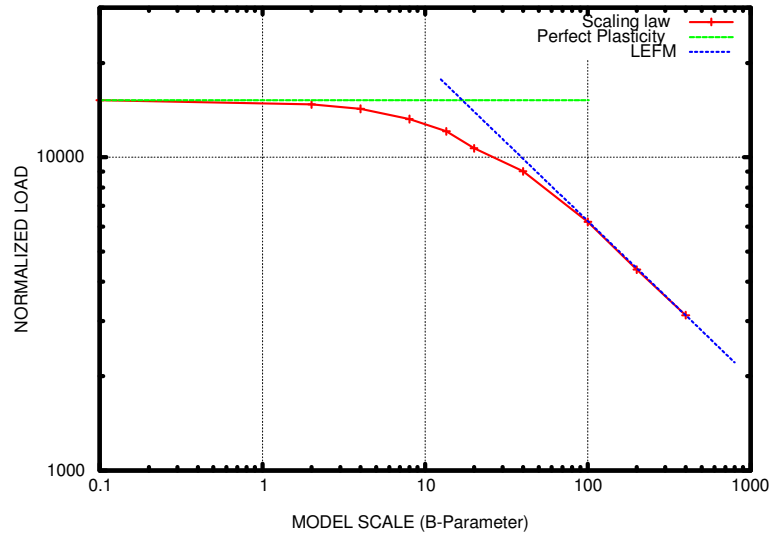

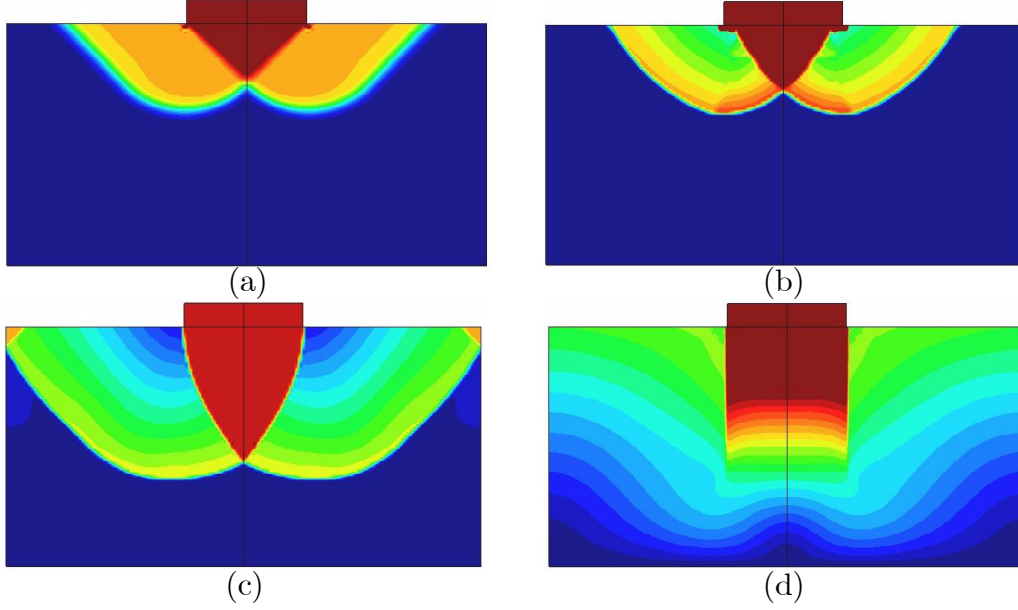Figure 11: Size effect on the nominal strength at failure for Prandtl's punch test

22

Figure 12: Displacement contour fills for the Prandtl's punch test with different scales: (a) $\Pi_B = 0$, (b) $\Pi_B = 4$, (c) $\Pi_B = 40$, (d) $\Pi_B = 100$

ate increasing scales the normalized curves show increasing brittleness. For $\Pi_B > 20$, the curve changes shape in relation with the smaller scales. This phenomenon, not observed in the previous example, is discussed below.

Size effect on the peak load of the punch test is demonstrated in Figure 11, which shows normalized peak load vs size in log scale. The general trend of the plot is the same as in the previous example, but the smoothness of the curve is broken by a subtle kink that can be observed for $\Pi_B = 20$.

The explanation for the change of shape in the curves of Figure 10 and the small kink in the curve of Figure 11 has to be sought in the solutions obtained for the different scales investigated. Figures 12 and 13 show displacement and equivalent plastic strain contour fills, respectively, obtained once the plastic flow is fully developed and the collapse mechanism can be appreciated. They show contours for different scales: (a) $\Pi_B = 0$, (b) $\Pi_B = 4$, (c) $\Pi_B = 40$ and (d) $\Pi_B = 100$.

These plots demonstrate a new feature of the size effect: in problems where the shear bands develop slowly and there is a large change in the stress field during the pre and post peak regimes, the collapse mechanism may depend to a large extent on the scale of the problem.
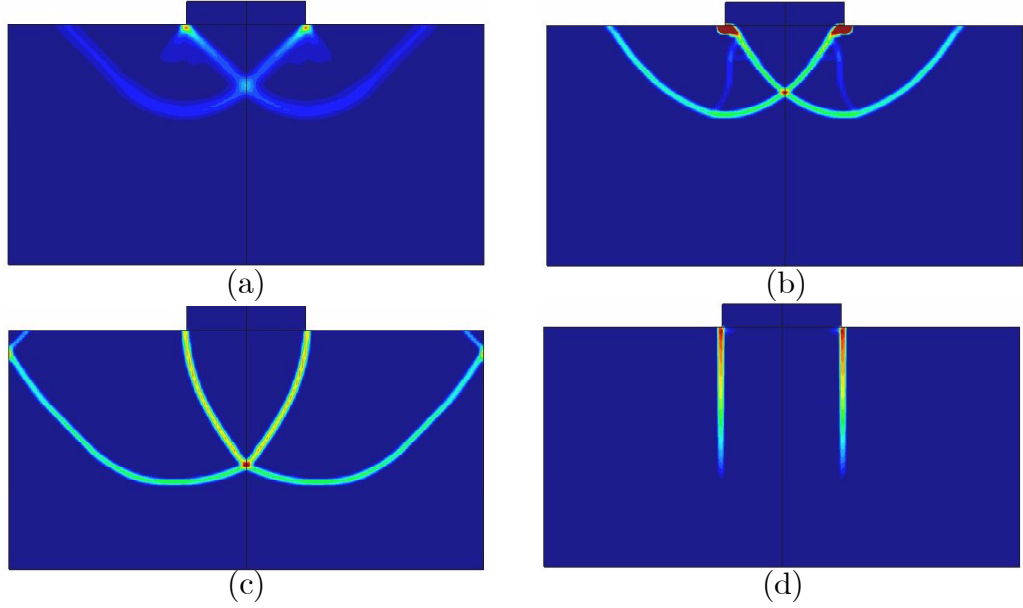
Figure 13: Equivalent plastic strain contour fills for the Prandtl's punch test with different scales: (a) $\Pi_B = 0$, (b) $\Pi_B = 4$, (c) $\Pi_B = 40$, (d) $\Pi_B = 100$

For the smallest scale, $\Pi_B = 0$, the solution obtained corresponds to the classical analytical solution for perfect plasticity: a straight shear band at 45° which starts at the singular point and that progresses in a circular arc before turning upwards to return to the top surface in a straight line exactly at 45°. This solution is not highly localized, as it can be observed in Figure 13a. For $\Pi_B = 4$, the solution changes slightly: the shear bands are much more sharply defined, the straight lines bend noticeably and the plastic zone expands downwards and outwards. For $\Pi_B = 20$, the plastic zone reaches the vertical lateral boundaries. For $\Pi_B = 40$, the change is very obvious and the "reflection" of the shear bands on the lateral boundaries can be appreciated. This is a fairly complex collapse mechanism. For $\Pi_B = 100$, the collapse mechanism is very different: the punch test has turned into a pure penetration test, with two vertical shear bands progressing downwards.

For all the scales, the orientation of the slip bands obtained is independent of the FE mesh used and the resolution is optimal: one element across. Results obtained using the standard irreducible $Q1$ element fail completely to model this problem and they are only able to represent the last case, where the slip lines follow the alignment of the mesh [44].
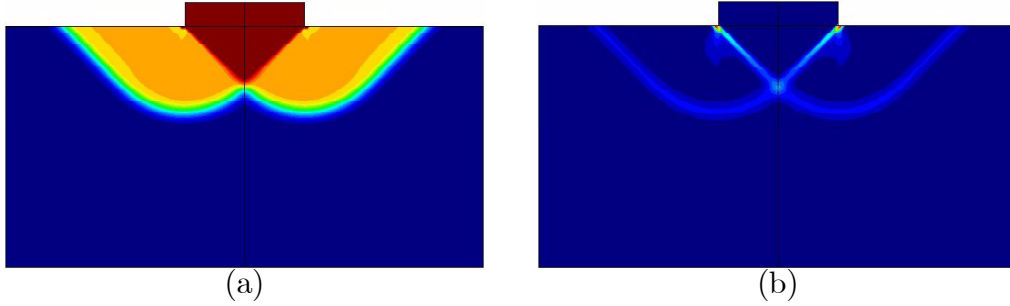
24

<div style="text-align:center">(a)   (b)</div>

Figure 14: Displacement and equivalent plastic strain contour fills for the Prandtl's punch test with P1P1 triangular elements ($\Pi_B = 0$)

As in the previous example, and in order to assess the validity of the solutions obtained, the problem is also solved using a second FE mesh. To this end, the quadrilateral elements of the mesh shown in Figure 9 are halved to obtain a structured mesh of 13,200 $P1P1$ stabilized triangles (6,771 nodes). Figure 14 shows results obtained using this second mesh for the smallest scale ($\Pi_B = 0$), once the collapse mechanism can be appreciated. This Figure shows contours for: (a) displacement and (b) equivalent deviatoric plastic strain. Again, the resemblance between this solution and the one obtained using the mesh of quadrilaterals is remarkable. Similar results are obtained using unstructured meshes of stabilized $P1P1$ triangular elements [44].

6 Conclusions

This paper presents the application of a stable mixed finite element formulation, written in terms of displacement and pressure fields, to the study of size effect in quasi-brittle failure involving shear slip lines. The procedure involves the use of a locally defined softening J2-plasticity model and the corresponding FE softening regularization.

The key point of the proposed formulation is to ensure stability of the resulting discrete FE formulation. To this end, two different FE strategies are followed. On one hand, $Q1P0$ quadrilaterals with continuous bilinear displacement and discontinuous constant pressure interpolations are used. This approach, (marginally) stable, is simple to implement in a standard FE code and it is very economical in computational terms. On the other hand, $P1P1$ triangles with equal continuous linear/linear displacement/pressure interpo-

<div style="text-align:center">25</div>

lations are used. This alternative approach, stabilized via the *orthogonal sub-grid scale method (OSGS)*, is more versatile and suitable for engineering applications in 2D and 3D.

Numerical examples demonstrate that the mixed displacement/pressure formulation is able to predict correct failure mechanisms with localized patterns of plastic deformation, which are practically free from any dependence of the mesh directional bias. Also, a stable formulation of the problem yields a satisfactory global response in the pre and post peak regimes. The concordance of the results obtained using the two different finite element strategies highlights the robustness of the proposed formulation.

Evaluating the structural response in two selected benchmarks, it can be concluded that the formulation proposed is able to solve a wide range of structural scales, including real life engineering applications. Furthermore, it includes the classical theories of perfect plasticity and linear fracture mechanics as limit cases.

7   Acknowledgments

References

[1] Galilei, G. (1638). Discorsi e dimonstrazioni matematiche intorno a due nuove scienze. English translation: Two new sciences, The Macmillan Company (1933), New York.

[2] Mariotte, E. (1686). Traité du movement des eaux. English translation: J. T. Desvaguliers (1718), London.

[3] Griffith, A.A. (1921). The phenomenon of rupture and flow of solids. Phil. Trans. Roy. Soc. (London), 22, 163-198.

[4] Bazant, Z. P. and Planas, J. (1198). Fracture and Size Effect in Concrete and Other Quasibrittle Materials. Boca Raton: CRC Press.

[5] de Borst, R. (1991). Simulation of strain localization: a reppraisal of the Cosserat continuum. Engineering Computations, 8, 317-322.

[6] Steinmann, P. and Willam, K. (1992). Localization witin the framework of micropolar elastoplasticy. In Advances in Continuum Mechanics. ed. V. Mannl et al. pp. 296-313. Springer Verlag, Berlin.

[7] Aifantis, E.C. (1984). On the microstructural origin of certain inelastic models. Transactions ASME Journal of Engineering Materials Technology, 106, 326-330.

[8] Vardoulakis, I. and Aifantis, E.C. (1991). A gradient flow theory of plasticity for granular materials. Acta Mechanica, 87, 197-217.

[9] de Borst, R. and Mulhaus, H.B. (1992). Gradient-dependent plasticity: formulation and algorithm aspect. Int. J.. Num. Meths. in Engng., 35, 521-539.

[10] Pamin, J. (1994). Gradient-Dependent Plasticity in Numerical Simulation of Localization Phenomena. Ph. D. Thesis, TU Delft, The Netherlands.

[11] Peerlings, R.H.J., de Borst, R., Brekelmans, W.A. M. and Geers, M.G.D. (1998). Gradient-enhanced damage modelling of concrete failures. Mechanics of Cohesive-Frictional Materials, 4, 339-359.

[12] Pijaudier-Cabot, G. and Bazant, Z.P. (1987). Nonlocal Damage Theory. Journal of Engineering Mechanics, ASCE, 113(10) 1512-1533.

[13] Pijaudier-Cabot, G. and Huerta, A. (1991). Finite Element Analysis of Bifurcation in Nonlocal Strain Softening Solids, Comp. Meth. in Applied Mech. and Engrg., 90, 905-919.

[14] Jirásek, M. (1998). Nonlocal models for damage and fracture: comparison of approaches. Int. J. Solids and Structures, 35, 4133-4145.

[15] de Borst, R. (2001). Some recent issues in computational failure mechanics. Int. J. Num. Meths. in Eng., 52, 63-95.

[16] Simo, J.C., Oliver, J. and Armero, F. (1993). An analysis of strong discontinuities induced by strain-softening in rate-independent inelastic solids. Computational Mechanics, 12, 49-61.

27

[17] Oliver, J. (1995). Continuum modeling of strong discontinuities in solid mechanics using damage models. Computational Mechanics, 17, 277-296.

[18] Oliver, J., Cervera, M. and Manzoli, O. (1999). Strong discontinuities and continuum plasticity models: the strong discontinuity approach. Int. J. of Plasticity, 15, 319-351.

[19] Belytschko, T. and Black, T. (1999). Elastic crack growth in finite elements with minimal remeshing. Comp. Meth. in Appl. Mech. and Eng., 45(5), 601-620.

[20] Möes, N., Dolbow, J. and Belytschko, T. (1999). A finite element method for crack growth without remeshing. Int. J. Num. Meths. in Engng., 46, 131-150.

[21] Sukumar, N., Möes, N., Moran, B. and Belytschko, T. (2000). Extended finite element method for three-dimensional crack modelling. Int. J. Num. Meths. in Engng., 48, 1549-1570.

[22] Guidault, P.A., Allix, O., Champaney, L. and Cornualt, C. (2008). A Multiscale eXtended Finite Element Method for crack propagation. Comp. Meth. in Appl. Mech. and Eng., 197, 381-399.

[23] Oliver, J., Huespe, A.E. Samaniego, E. and Chaves, W.V.. (2004). Continuum approach to the numerical simulation of material failure in concrete. Int. J. for Num. and Anal. Meth. in Geomechanics.,28, 609-632.

[24] Oliver, J. and Huespe, A.E. (2004). Continuum approach to material failure in strong discontinuity settings. Comp. Meth. in Appl. Mech. and Eng., 193, 3195-3220.

[25] Mosler, J. and Meschke, G. (2004). Embedded crack vs. smeared crack models: a comparison of elementwise discontinuous crack path approaches with emphasis on mesh bias. Comp. Meth. in Appl. Mech. and Eng., 193, 3351-3375.

[26] Wells, G.N., Sluys, L.J. and de Borst, R. 2002. A p-adaptive scheme for overcoming volumetric locking during plastic flow. Comp. Meth. in Appl. Mech. and Eng., 191, 3153-3164.

[27] Zienkiewicz, O.C. and Taylor, R.L., 2000. The Finite Element Method, Butterworth-Heinemann, Oxford.

[28] Zienkiewicz, O.C., Pastor, M. and Huang, M., 1995. Softening, localization and adaptive remeshing: capture of discontinuous solutions. Comp. Mech., 17, 98-106.

[29] Zienkiewicz O.C., Huang, M. and Pastor, M., 1995. Localization problems in plasticity using finite elements with adaptive remeshing. Int. J. Num. Methods in Geomechanics, 19, 127-148.

[30] Pastor, M., Li, T., Liu, X. and Zienkiewcz, O.C., 1998. Stabilized linear triangles for failure problems in undrained soils. Proceedings of IV World Congress on Computational Mechanics: "*Computational Mechanics: New Trends and Applications*", S. Idelshon, E. Oñate and E. Dvorkin (eds.), CIMNE, Barcelona, Spain.

[31] Pastor, M., Li, T., Liu, X., Zienkiewcz, O.C. and Quecedo, M., 2000. A fractional step algorithm allowing equal order interpolation for coupled analysis of saturated soil problems. Mechanics of Cohesive-Frictional Materials, 5, 511-534.

[32] Bonet, J. and Burton, A.J., 1998. A simple average nodal pressure tetrahedral element for incompressible and nearly incompressible dynamic explicit applications. Comm. Num. Meths. in Eng., 14, 437-449.

[33] Zienkiewicz, O.C., Rojek, J., Taylor, R.L. and Pastor, M., 1998. Triangles and tetrahedra in explicit dynamic codes for solids, Int. J. for Num. Meths. in Eng., 43, 565-583.

[34] Klaas, O., Maniatty, A. and Shephard, M.S., 1999. A stabilized mixed finite element method for finite elasticity. Formulation for linear displacement and pressure interpolation, Comp. Meth. in Appl. Mech. and Eng., 180, 65-79.

[35] Taylor, R.L. A mixed formulation for triangular and tetrahedral elements, In Abascal, R., Domínguez, J. and Bugeda, G., editors, Conference Proceedings on *Métodos Numéricos en Ingeniería,* SEMNI, Barcelona, Spain, 1999.

[36] Dohrmann, C.R., Heinstein, M.W., Jung, J., Key, S.W. and Witkowsky, W.R., 2000. Node-based uniform strain elements for three-node triangular and four-node tetrahedral meshes. Int. Jour. for Num. Meths. in Eng. 47, 1549-1568.

[37] Taylor, R.L., 2000. A mixed-enhanced formulation for tetrahedral elements. Int. Jour. for Num. Meths. in Eng. 47, 205-227.

[38] Bonet, J., Marriot, H. and Hassan, O., 2001. An averaged nodal deformation gradient linear tetrahedral element for large strain explicit dynamic applications. Comm. Num. Meths. in Eng., 17, 551-561.

[39] Bonet, J., Marriot, H. and Hassan, O., 2001. Stability and comparison of different linear tetrahedral formulations for nearly incompressible explicit dynamic applications. Int. Jour. for Num. Meths. in Eng., 50, 119-133.

[40] Oñate, E., Rojek, J., Taylor, R.L. and Zienkiewicz, O.C. Linear triangles and tetrahedra for incompressible problem usung a finite calculus formulation, Proceedings of European Conference on Computational Mechanics, ECCM, Cracow, Poland, 2001.

[41] de Souza Neto, E.A., Pires, F.M.A. and Owen D.R.J. A new F-bar-method for linear triangles and tetrahedra in the finite strain analysis of nearly incompressible solids. Proceedings of VII International Conference on Computational Plasticity, COMPLAS, Barcelona, Spain, 2003.

[42] Chiumenti, M., Valverde, Q., Agelet de Saracibar, C. and Cervera, M., 2002. A stabilized formulation for incompressible elasticity using linear displacement and pressure interpolations, Comp. Meth. in Appl. Mech. and Eng., 191, 5253-5264.

[43] Cervera, M., Chiumenti, M., Valverde, Q. and Agelet de Saracibar, C. 2003. Mixed Linear/linear Simplicial Elements for Incompressible Elasticity and Plasticity. Comp. Meth. in Appl. Mech. and Eng., 192, 5249-5263.

[44] Cervera, M., Chiumenti, M. and Agelet de Saracibar, C. 2003. Softening, localization and stabilization: capture of discontinuous solutions in J2 plasticity. Int. J. for Num. and Anal. Meth. in Geomechanics, 28, 373-393.

[45] Cervera, M., Chiumenti, M. and Agelet de Saracibar, C. 2003. Shear band localization via local J_2 continuum damage mechanics. Comp. Meth. in Appl. Mech. and Eng., 193, 849-880.

[46] Chiumenti, M., Valverde, Q., Agelet de Saracibar, C. and Cervera, M., 2004. A stabilized formulation for incompressible plasticity using linear triangles and tetrahedra, Int. J. of Plasticity, 20, 1487-1504.

[47] Agelet de Saracibar, C., Chiumenti, M., Valverde, Q. and Cervera, M., 2006. On the orthogonal subgrid scale pressure stabilization of finite deformation J_2 plasticity. Comp. Meth. in Appl. Mech. and Eng., 195, 1224-1251.

[48] Buckingham, E. (1914). On Physically Similar Systems: Illustrations of the Use of Dimensional Analysis. Phys. Rew., 4, 345-376.

[49] Simo, J.C. and Hughes, T.J.R. 1998. Computacional Inelasticity. Interdisciplinary Applied Mathematics. Vol. 7. Springer.

[50] Bazant, Z.P. and Oh, B.H. (1983). Crack band theory for fracture of concrete. Material and Structures, 16, 155-177.

[51] Rots, J.G., P. Nauta, G.M.A. Kusters and J. Blaauwendraad (1985). Smeared Crack Approach and Fracture Localization in Concrete. Heron 30 (1).

[52] Oliver, J., 1989. A consistent characteristic length for smeared cracking models. Int. J. Num. Meth. Engng., 28, 461-474.

[53] Brezzi, F. and Fortin, M., 1991. Mixed and Hybrid Finite Element Methods, Spinger, New York.

[54] Hughes, T.J.R., 1995. Multiscale phenomena: Green's function, Dirichlet-to Neumann formulation, subgrid scale models, bubbles and the origins of stabilized formulations, Comp. Meth. in Appl. Mech. and Eng., 127, 387-401.

[55] Hughes, T.J.R., Feijoó, G.R., Mazzei. L., Quincy, J.B., 1998. The variational multiscale method-a paradigm for computational mechanics, Comp. Meth. in Appl. Mech. and Eng., 166, 3-28.

[56] Codina, R. and Blasco, J., 1997. A finite element method for the Stokes problem allowing equal velocity-pressure interpolations, Comp. Meth. in Appl. Mech. and Eng., 143, 373-391.

[57] Codina, R., 2000. Stabilization of incompressibility and convection through orthogonal sub-scales in finite element methods, Comp. Meth. in Appl. Mech. and Eng., 190, 1579-1599.

[58] Hughes, T.J.R. 2000. The Finite Ewlement Method: Linear Static and Dynamic Finite Element Analysis. Dover.

[59] Cervera, M., Agelet de Saracibar, C. and Chiumenti, M., 2002. COMET: COupled MEchanical and Thermal analysis. Data Input Manual, Version 5.0, Technical report IT-308, www.cimne.upc.es.

[60] GiD: the personal pre and post processor, 2008. www.gidhome.com.